

A refractory Ca–SiO–H₂–O₂ vapor condensation experiment with implications for calciosilica dust transforming to silicate and carbonate minerals

Frans J.M. Rietmeijer^{a,*}, Aurora Pun^a, Yuki Kimura^b, Joseph A. Nuth III^c

^a Department of Earth and Planetary Sciences, MSC03-2040, University of New Mexico, Albuquerque, NM 87131-0001, USA

^b Laboratory for Nano-Structure Science, Department of Physics, Ritsumeikan University, 1-1-1 Nojihigashi, Kusatsu-shi, Shiga, 525-8577, Japan

^c Astrochemistry Laboratory, Solar System Exploration Division, Code 691, NASA Goddard Space Flight Center, Greenbelt, MD 20771, USA

Received 6 March 2007; revised 3 August 2007

Available online 23 December 2007

Abstract

Condensates produced in a laboratory condensation experiment of a refractory Ca–SiO–H₂–O₂ vapor define four specific and predictable deep metastable eutectic calciosilica compositions. The condensed nanograins are amorphous solids, including those with the stoichiometric CaSiO₃ pyroxene composition. In evolving dust-condensing astronomical environments they will be highly suitable precursors for thermally supported, dust-aging reactions whereby the condensates form more complex refractory silicates, e.g., diopside and wollastonite, and calcite and dolomite carbonates. This kinetically controlled condensation experiment shows how the aging of amorphous refractory condensates could produce the same minerals that are thought to require high-temperature equilibrium condensation. We submit that evidence for this thermal annealing of dust will be the astronomical detection of silica (amorphous or crystalline) that is the common, predicted, by-product of most of these reactions.

© 2007 Elsevier Inc. All rights reserved.

Keywords: Comets; dust; Disks; Mineralogy; Experimental techniques

1. Introduction

Many astronomical environments (see Molster and Waters, 2003 for a review) and active comets (Sitko et al., 2004; Harker et al., 2005; Lisse et al., 2006, among others) contain a rich variety of minerals. They include (1) amorphous dusts with an Mg-rich olivine or pyroxene silicate composition, (2) forsterite [Mg₂SiO₄] and enstatite [MgSiO₃] minerals that are the crystalline forms of these amorphous silicates, (3) fayalite [Fe₂SiO₄] and ferrosilite [FeSiO₃] minerals, (4) SiO₂ (Molster and Waters, 2003), (5) Ca-rich pyroxene [diopside, MgCaSi₂O₆], and (6) carbonates. The latter are mostly calcite [CaCO₃] and dolomite [MgCa(CO₃)₂] around protostars and in O-rich planetary nebulae (Molster and Waters, 2003; Chiavassa et al., 2005). Magnesite–siderite [MgCO₃–FeCO₃] carbonates could be among the Comet Tempel 1 dust (Lisse et

al., 2006, 2007). Magnesite is found in an anhydrous interplanetary dust particle (IDP) (Rietmeijer, 1990). Magnesite–siderite carbonates co-occur with the layer silicate mineral saponite [Mg₃Si₂O₅(OH)₄] in hydrated IDPs (see Rietmeijer, 1998 for a review). With the exception of young stars and the ISM, amorphous and crystalline Mg-silicates are ubiquitous (Molster and Waters, 2003; Lisse et al., 2006; Sitko et al., 2004; Harker et al., 2005, among others). Thermal processing of amorphous silicates could lead to the formation of crystalline silicates, which is considered to be a dust-aging process (e.g., Nuth and Hecht, 1990; Hallenbeck et al., 1998; Nuth et al., 2000a; Bouwman et al., 2001; Hill et al., 2001). The enormously varied Comet 81P/Wild 2 minerals include refractory minerals such as diopside, and the CaAl-silicates plagioclase (CaAl₂Si₂O₈) and gehlenite (Ca₂Al₂SiO₇) (Zolensky et al., 2006) that are common minerals in Calcium–Aluminum-rich Inclusions (CAIs) in carbonaceous chondrite meteorites (see Brearley and Jones, 1998 for a review). Crystals of Ca-oxide (>100 nm) are found as inclusions in some refractory CAI minerals and could be pri-

* Corresponding author.

E-mail address: fransjmr@unm.edu (F.J.M. Rietmeijer).

many condensates (Greshake et al., 1998). These CAI minerals are also found in rare refractory IDPs (Zolensky, 1987) while diopside and amorphous CaMg-bearing aluminosilica grains occur in anhydrous aggregate IDPs (Rietmeijer, 1998, 1999).

Vapor phase condensation in supernovae and AGB atmospheres and winds is the widely accepted dust-forming process that produces amorphous or crystalline materials, and sometimes both. Binary solids such as oxides (e.g., MgO, SiO₂, Al₂O₃, CaO), carbides and nitrides (Kozasa and Sogawa, 1997; Rietmeijer, 1988, 1992; Molster and Waters, 2003) could form crystalline dust due to equilibrium gas-to-solid condensation. The condensation of complex solids would likely favor the amorphous state.

The crystallographic state of dust will determine its response during post-condensation agglomeration and thermal processing to bigger, more chemically complex grains that might eventually come to resemble stoichiometric minerals such as those that were predicted by equilibrium condensation models (Grossman and Larimer, 1974; Wood and Hashimoto, 1993; Fegley, 2000, among many others). Equilibrium condensation describes the stability of ordered, chemically stoichiometric solids, that is, minerals, as a function of temperature (at fixed pressure) and composition of a fractionating vapor (Wood, 1988; Grossman and Larimer, 1974). The obvious problem with non-equilibrium condensation is that neither the crystallographic and chemical condensate properties nor an orderly condensation sequence can be readily predicted. Yet, kinetic factors in natural environments will ensure non-equilibrium vapor phase condensation. The system then becomes chaotic. This condition might change when condensation occurs sufficiently far removed from thermodynamic equilibrium with the emergence of a new state of matter where extreme disorder becomes a metastable state, i.e., a dissipative structure (Prigogine, 1978, 1979). De (1979) suggested that dissipative structures arise during vapor phase condensation under astronomical conditions.

That is, during vapor phase condensation before the gas and grain temperatures become equal (i.e. equilibrium condensation), there will be an initial regime wherein condensation exceeds evaporation, or vice versa. Environmental conditions could allow “capturing” the evolving kinetic system when condensation exceeds evaporation, thus producing condensates during the chaotic phase of the overall condensation process. The highly disordered state of these solids in fact becomes a transient state of matter. In this property they resemble the dissipative structures formulated by Prigogine (1978, 1979). One could ask what such dissipative structures might look like, or even if they could be understood in terms of known phase relationships. A eutectic point is a common temperature–composition feature in binary equilibrium phase diagrams (Fig. 1). This hypothetical equilibrium phase diagram showing the phase compositions *A* and *B* vs temperature on the vertical axis has two eutectic points where the liquidus has two minima. From each of these points it is possible to extend the stable liquidus (solid) line to a lower temperature (dashed lines) until they intersect at a (deep) metastable eutectic point. Its “*AB*” composition arises when cooling is extremely rapid preventing equilibrium to be achieved. There are no thermody-

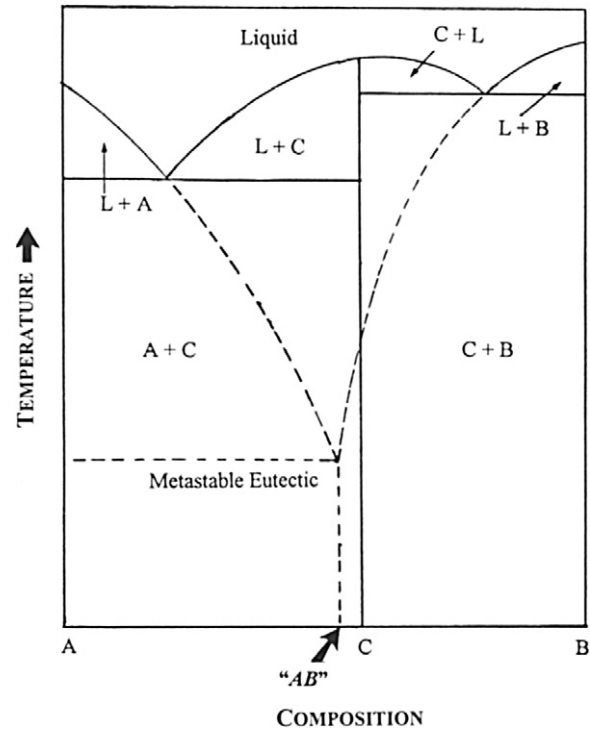


Fig. 1. A hypothetical binary equilibrium phase diagram between the compositional end-members *A* and *B* as a function showing the position of the (deep) metastable eutectic point with the “*AB*” composition defined at the intersect of the metastable extensions of the liquidus surface (dashed lines) located in between the compositions of both (stable) eutectic points on the liquidus surface at the top of the diagram (solid lines). Modified after Rietmeijer and Nuth (2000); courtesy of the American Geophysical Union.

amic arguments that would forbid such DME points to exist (Aasland and McMillan, 1994; Highmore and Greer, 1989) but they will not have predictable temperatures because of the kinetic conditions required for this behavior to emerge. Yet, the chemical composition (“*AB*” in Fig. 1) of the DME point will always be positioned in between two stable eutectic points.

A series of kinetically controlled vapor phase condensation experiments using Mg–Fe–SiO–H₂–O₂, Mg–SiO–H₂–O₂, Fe–SiO–H₂–O₂ and Al–SiO–H₂–O₂ vapors systematically yielded highly disordered amorphous nanograins with deep metastable eutectic (DME) compositions (Nuth et al., 2000b, 2000c; Rietmeijer et al., 2004). They are the predicted dissipative structures. It follows that natural condensation will produce simple stoichiometric oxide nanograins and amorphous non-stoichiometric mixed silicate nanograins. Larger, chemically complex amorphous grains will be the result of agglomeration and fusion of DME condensate grains (Rietmeijer et al., 2006). Experimental verification of natural mineral-forming processes can be a very powerful tool to elucidate the processes in natural environments that are inaccessible to direct sampling or wherein the processes occur over long time scales (Rietmeijer and Nuth, 2002). The compositions of MgFeSiO units in aggregate IDPs and many of the Comet Halley silicate particles are matched by amorphous agglomerates of fused magnesiosilica and ferrosilica dust condensates with DME compositions (Rietmeijer, 2002;

Rietmeijer and Nuth, 2004). This example shows how these laboratory condensation experiments can make testable predictions of natural dust compositions.

As the condensation of grains with a DME composition requires the presence of at least two stable eutectic points (Fig. 1), the number of amorphous solids each with a DME composition is then entirely constrained by the number of stable eutectics in the phase diagram. In the metal-oxide/silica systems studied so far, vapor phase condensation systematically produced amorphous condensates with three distinct DME compositions, viz.

- (1) Smectite dehydroxylate: $M_6\text{Si}_8\text{O}_{22}$,
- (2) Serpentine dehydroxylate: $M_3\text{Si}_2\text{O}_7$, and
- (3) Very low-Si, $M\text{SiO}$,

wherein M can be Mg, Fe, or Al (Nuth et al., 1999, 2000b, 2000c; Rietmeijer et al., 1999a, 1999b, 2002a, 2006). The names for the solids (1) and (2) refer to M/Si ratios that are those of smectite and serpentine layer silicate minerals, respectively, but with the structural layer silicate $(\text{OH})^-$ groups replaced by O^{2-} . An important implication of kinetically controlled vapor phase compositions is that invariably the condensates will have all possible DME compositions. The molecules in a condensing gas will form molecular clusters that eventually form the smallest nanograins detectable by transmission electron microscopes, which in our case is ~ 2 nm, mostly as a consequence of the embedding technique used for ultrathin section preparation.

We report here on Si-oxide and calciosilica grains formed in a condensing Ca–SiO–H₂–O₂ vapor produced by mixing simple vapor molecules. We have only hints to the compositions of the molecular clusters and sub-nanometer solids forming in the vapor that were the precursors to the first (recognizable) nanometer-sized condensates that grew by solid–solid, solid–gas, liquid–gas, or all three, reaction mechanisms. We found that the amorphous calciosilica grains had all of the anticipated DME compositions. For the first time in our experiments, the amorphous condensates included a stoichiometric mineral composition, that is CaSiO₃, which will have implications for Ca-silicate minerals in O-rich dust-forming environments.

2. Experimental procedures

Laboratory condensation of a silica-saturated Ca–SiO–H₂–O₂ vapor was conducted in the Condensation Flow Apparatus (CFA) at the NASA Goddard Space Flight Center (Nelson et al., 1989; Nuth et al., 2000b, 2000c, 2002). During a condensation experiment we define two distinct regimes: (1) vapor condensation *proper*: e.g. smoke formation, and (2) autoannealing of grains, probably in the gas phase before they settled onto the collector surfaces placed inside the CFA (Rietmeijer and Nuth, 1991). Autoannealing is an experimental artifact related to the heat dissipation in a contained experiment. Recognizing this process will allow recognizing the condensation process *proper* (Nuth et al., 1999, 2000b). In the laboratory we cannot duplicate the exact conditions that lead to and will deter-

mine vapor condensation in astronomical settings but we can study the fundamental properties of the process, such as the DME behavior. Separating the processes of these two regimes occurring in the experiments allows tracking the effects of condensation proper and the initial phases of thermal annealing, referred to as autoannealing (Rietmeijer and Nuth, 1991; Rietmeijer et al., 2002b).

Condensates were produced in a hydrogen-dominated atmosphere at ~ 80 Torr total pressure at furnace temperatures of around 1100 K. The hydrogen flow rate was maintained at ~ 500 standard cubic centimeters per minute (sccm). Ca-metal (Alfa Aesar, A Johnson Matthey Company, 99%) was placed in a graphite ‘boat’ inside an alumina furnace tube to produce calcium vapor. At the furnace temperature chosen for these experiments, Ca metal has a vapor pressure of ~ 1 Torr. Silane (SiH₄) was added to the vapor mixture at the same flow rates as oxygen, between 30 and 500 sccm. The silane and hydrogen gases passed through a mixing chamber before entering the furnace (Nuth et al., 2002). The grains formed while passing through a hydrogen–oxygen flame-front in the furnace before exiting the alumina furnace tube (maintained at 1100 K) and passing into a larger region of cooler gas (~ 400 K). The condensates deposited onto an aluminum collector that had a nominal temperature around 400 K and that is the effective quench temperature for the condensed dust. Dust was carefully removed and placed in clean vials for shipment. A small amount of this smoke was removed from the vials and placed in a clean mortar. Gentle pressure was applied to crush the blocky smoke deposit. This powder was embedded in epoxy (Spurrs) following standard procedures in the Electron Microbeam Analysis Facility at UNM. Serial ultrathin (70 nm) sections were cut from epoxy stubs with embedded smoke material. The sections were placed on a thin holey carbon film supported by 200 mesh standard TEM Cu grids for analyses using a JEOL 2010 high-resolution transmission electron microscope (HRTEM) that operated at a 200 keV accelerating voltage and was equipped with a LINK ISIS energy dispersive spectrometer (EDS) with an ultrathin-window for *in situ* quantitative chemical analyses, including oxygen, using the standard Cliff–Lorimer thin film (Cliff and Lorimer, 1975) procedure. The analytical spot size used on individual grains was 10 nm. The reported oxide values have a 2% relative error. Selected area electron diffraction analysis was used to determine the crystallographic properties of each grain. For grains smaller than the ultrathin section thickness we applied a through-focus technique to determine the shapes below the section surface. A slow-scan CCD is capable of on-line and low-dose TEM imaging. Grain sizes were measured in computer-stored images with a relative error of $\sim 10\%$.

3. Observations

The bulk composition of all condensed solids, SiO₂ = 65 wt% and CaO = 35 wt%, is considered a proxy for the bulk composition of the condensing Ca–SiO–H₂–O₂ vapor. The procedure to obtain this composition tends to somewhat underestimate the amount of silica in the vapor because we have not analyzed all of the pure silica grains. Their chemistry is not

of prime interest to this study. Most of the condensed smoke is a highly open, i.e. porous material of individual calciosilica (CaSiO) grains that are arranged in short chains and clusters of variable porosity. Typically massive CaSiO grains have a rounded to subhedral shape and tend to form small clusters in a highly porous smoke (Fig. 2). Interlaced and tangled chains of pure silica (SiO₂) grains (Fig. 3) are interspersed among these calciosilica grain structures. All condensed grains are amorphous irrespective of their composition. The silica and calciosilica grain sizes (Table 1) define lognormal size distributions (log size vs cumulative percent) that is typical for size sorting when larger grains are continuously formed by coagu-

lation and fusion of smaller grains. The CaSiO grains form two normal distributions with a discontinuity at 60–65 nm. Bimodal size distributions are a typical feature in our experiments. The grains from the population smaller than the discontinuity represent the dust condensed directly from the gas phase. These condensates include one population of pure silica grains and four different populations of mixed calciosilica grains (Table 2).

The Student's t-test applied to the size distributions for each of these four populations of calciosilica grain compositions indicates that there is no reason to suggest that they are from populations having different mean grain sizes. That is, the condensate grain size increased independent of the atomic Ca/Si ratio. The observed calciosilica dust compositions are shown in

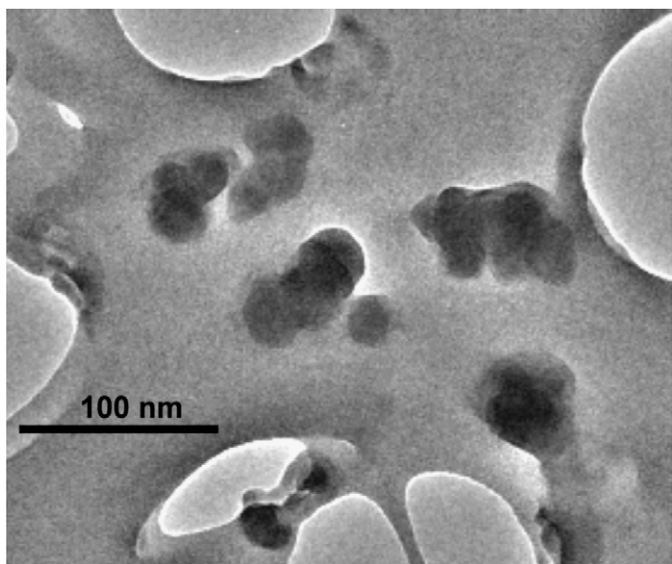


Fig. 2. Transmission electron microscope image of an ultrathin section of the highly porous calciosilica smoke that consists of small dense clusters of individual calciosilica condensate grains. The background shows the holey carbon thin-film that supports the section during analysis.

Table 1

Size (nm) of individual silica and calciosilica grains. All Gaussian distributions are defined at the 95% confidence limit

	Pure silica	Calciosilica grains	
Mean	13.5	33	84
Standard deviation	3.7		
Range	8–21	18–62	65–118
Number of grains	99	334	23

Table 2

CaO (wt%) contents of smoke grains condensed from a Ca–SiO–H₂–O₂ vapor. The bottom row values are a qualitative measure for the relative proportions of the grain populations

	Pure silica	Calciosilica grains			
Population		I	II	III	IV
Mean	0	9	42	72	87
Standard deviation	n.a.	3	4	5.5	4
Range	n.a.	1–17.5	36–50	60–80	80–97
Number of grains	95	42	23	46	50

Note. The Gaussian distributions for calciosilica grains are at the 95% confidence limit; n.a.: not applicable.

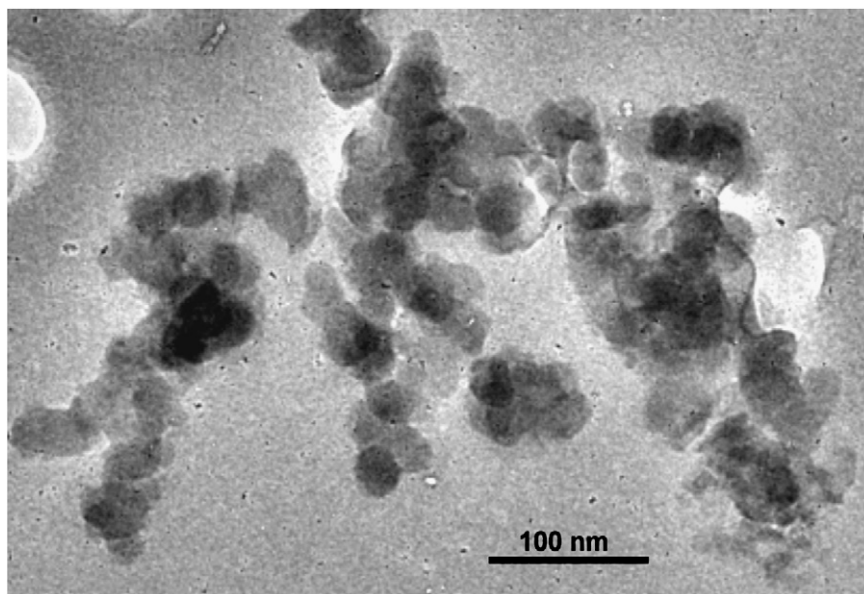


Fig. 3. Transmission electron microscope image of an ultrathin section showing of several chains of Si-oxide grain condensates present among the calciosilica grains condensed from the Ca–SiO–H₂–O₂ vapor. These chains are typical for samples produced by vapor phase condensation.

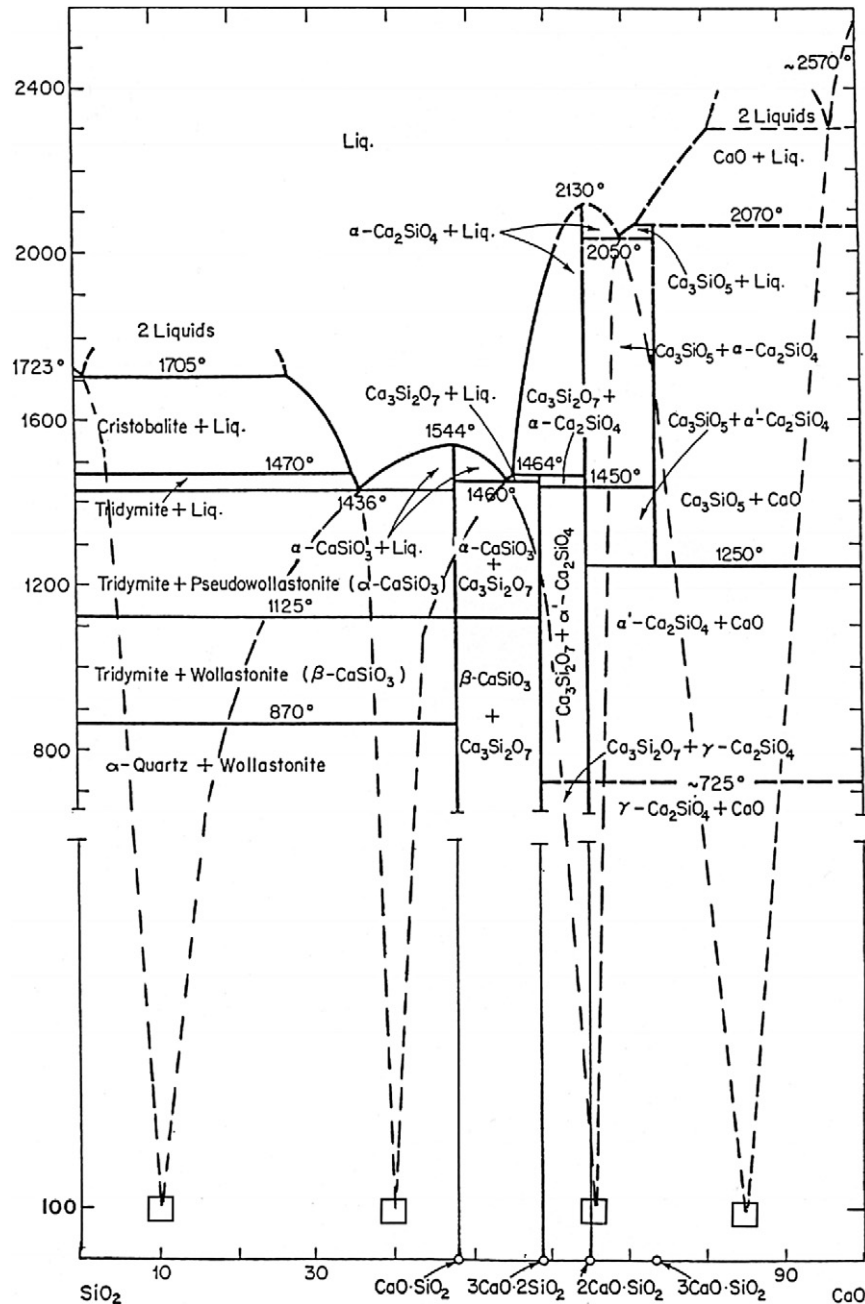


Fig. 4. The CaO–SiO₂ phase diagram [wt% oxides vs temperature (°C)] modified after Ehlers (1972) showing four deep metastable eutectic points (open squares). The original liquidus boundary on the CaO side of the diagram is modified to include a high-silica CaSiO eutectic point (cf. Rietmeijer and Karner, 1999; Rietmeijer et al., 1999a, 1999b, 2002a). We stress that a deep metastable eutectic (DME) point cannot have a unique position in an equilibrium temperature–composition phase diagram. Their positions shown here are based on the nominal quench temperature (~100 °C) and the measured grain compositions.

the CaO–SiO₂ phase diagram noticing there are no pure Ca-oxide condensate grains (Fig. 4).

We also made semi-quantitative oxygen measurements of the condensed grains that are plotted in the Si–Ca–O (atomic) diagram (Fig. 5). These data show

- (1) Si₂O₃ metasilicate; Si = 39 ± 4.7 (mean ± 1σ; range = 33–48) and O = 61 ± 2.6 (range = 52–66),
- (2) Stoichiometric silica (SiO₂); Si = 33 (range = 30–34) and O = 67 (range = 65–70),
- (3) One, almost pure metallic Ca_{0.1}Si_{0.9} alloy grain; O = 3.5.

Stoichiometric silica is a common condensate in our silicate smokes. The oxygen measurements also indicate the metasilicate phase and a slightly oxidized Si, Ca-alloy composition. The bulk composition of the condensing vapor is Ca:Si:O (atomic) = 17:25:58.

4. Discussion

The discontinuity in the bimodal grain size distributions, 60–65 nm, is higher than the 20–30 nm range typically seen in aluminosilica (Rietmeijer and Karner, 1999), magnesiosil-

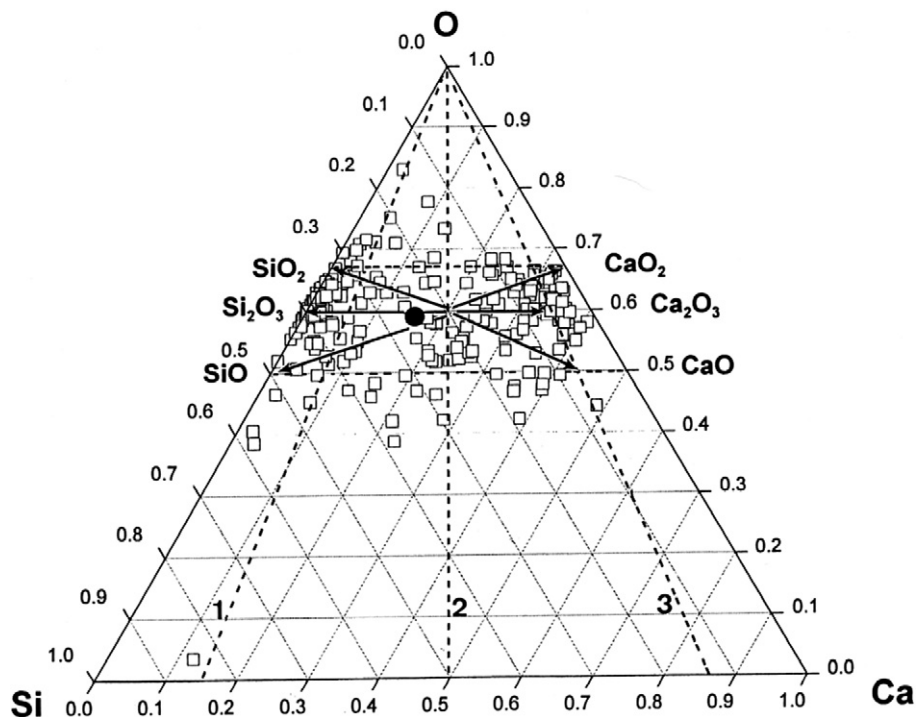


Fig. 5. The Si–Ca–O (atomic) diagram showing the compositions for 252 individual grains that condensed from a Ca–SiO–H₂–O₂ vapor. The calculated bulk vapor composition (black dot) is close to a calcium disilicate, CaSi₂O₅, composition. The mixing lines 1–3 between the deep metastable eutectic Ca,Si alloys and oxygen constrain Ca/Si ratios of calciosilica grain compositions. The arrows indicate the directions of reactions between the CaSiO₃ and the Si- and Ca-oxides that led to the deep metastable eutectic condensate compositions (see Fig. 2).

ica (Rietmeijer et al., 2002a) and ferrosilica (Rietmeijer et al., 1999a) smokes. It probably reflects the higher (~1100 K) temperature of refractory Ca–SiO–H₂–O₂ vapor compared to the lower temperatures in these previously studied vapor systems. The smallest, typically amorphous, condensed grains in these smokes have the compositions of the predictable deep metastable eutectic points in their equilibrium phase diagrams. The five stable eutectic points in the CaO–SiO₂ phase diagram (Ehlers, 1972) predict four possible deep metastable eutectic points, viz. at ~10, ~40, ~65 and ~85 CaO wt% (Fig. 4). The measured calciosilica condensate compositions (Table 2) closely resemble these predicted DME compositions. These refractory calciosilica grains are also highly disordered, amorphous nanograins that will be highly reactive when responding to changes in their physiochemical environments.

The Si₂O₃ metasilicate and stoichiometric silica in this condensation experiment are predicted by the Si–SiO₂ phase diagram of Sosman (1955) that at low pressure has a SiO gas molecule and a metastable eutectic (SiO + SiO₂) solid composition. These phases were also found in a rapidly cooled SiO–H₂ vapor wherein SiO molecules that nucleated in the gas phase condensed as Si₂O₃ metasilicate (Nuth and Donn, 1982, 1984). A mixture of Si₂O₃ and amorphous SiO₂ formed at high temperatures. Amorphous SiO₂ probably formed by oxidation, or annealing, of less stable vapor clusters once deposited on the collector (Nuth and Donn, 1982, 1984). In the present study there were no pure Ca-oxides although CaO is a stable phase (Okamoto, 2001). Kimura and Nuth (2005), who used the same CFA facility for another Ca–SiO–H₂–O₂ vapor condensation

experiment, reported that condensed CaO nanograins reacted rapidly to Ca(OH)₂ when exposed to moisture. Since condensation in the CFA takes place in an O₂/H₂ atmosphere and SiO is formed from SiH₄, it is possible that water vapor produced in a reaction such as



and followed by



could form the hydroxide.

For the sake of argument, and knowing that the EDS detector used cannot measure hydrogen, this grain composition when rewritten as CaO₂H₂ shows that the detector will identify such grains as CaO₂. We believe that this explains the 1:2 Ca/O ratios observed in these oxides (Fig. 5).

Calcium vapor was produced from Ca-metal, which gives significance to the single surviving alloy composition detected that failed to fully react with oxygen either during condensation or after removal from the system. This particular alloy composition suggests that phase relationships in the Si–Ca (atomic) diagram could sometimes be critical in assessing condensation in Ca–SiO–H₂–O₂ vapors. This phase diagram was explored using a standard quenched-liquid technique but uncertainties remain with regard to the exact phase relationship as signified by dashed phase boundaries in its Ca-rich part (Wynnyckyj, 1972; Wynnyckyj and Pidgeon, 1972). Our interpretation of the data by Wynnyckyj and Pidgeon (1972) suggests that there is a stable eutectic that is slightly Si-rich from Ca₂Si in the Si–Ca

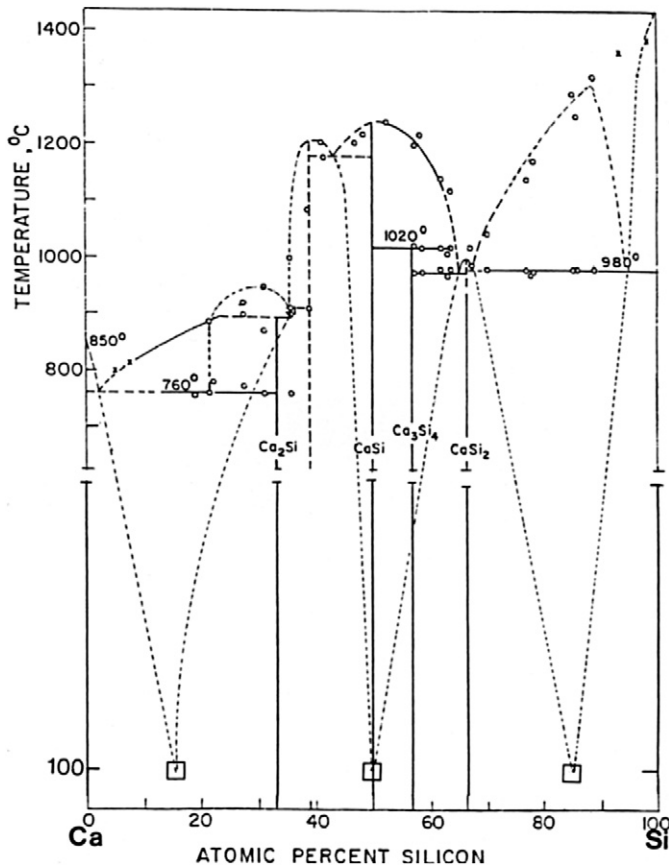


Fig. 6. The Si–Ca (atomic) phase diagram modified after Wynnyckyj and Pidgeon (1972) using the original experimentally determined data (open circles) and the correct silicon melting temperature of 1430 °C. The predicted CaSi alloy deep metastable eutectic points (open squares) are shown at ~ 0.15 , ~ 0.5 and ~ 0.85 atomic percent Si and the nominal quench temperature (100 °C) used in our experiment (see caption of Fig. 3).

Table 3

Ca/(Ca + Si) atomic ratios of deep metastable eutectic alloy and oxide compositions, and their approximate chemical formula, that are predicted from phase diagrams and observed calciosilica compositions

Alloys	Oxides
~ 0.15 (CaSi ₆)	~ 10
~ 0.5 (CaSi)	~ 40 (Ca ₆ Si ₈ O ₂₂ smectite dehydroxylate)
~ 0.85 (Ca ₆ Si)	~ 65 (larnite, Ca ₂ SiO ₄)
	~ 85

phase diagram. Assuming we are correct about six stable eutectic points (Fig. 6), we predict three Ca,Si-alloy DME points at Ca/(Ca + Si) (atomic) (1) ~ 0.15 (CaSi₆), (2) ~ 0.5 (CaSi) and (3) ~ 0.85 (Ca₆Si) (Fig. 6).

There are three deep metastable eutectic alloy (i.e. Ca,Si-phases) compositions but four calciosilica DME compositions in the CaO–SiO₂ phase diagram (Table 3). If the alloys reacted with oxygen than this would explain the formation of the calciosilica condensates that stretch along mixing lines 1–3 (Fig. 5). This would explain the dearth of pure Ca-oxides. There should have been many condensed grains with calciosilica compositions along mixing line 2 between the alloy with Ca/(Ca + Si) = 0.6 and the oxygen apex of the diagram. In-

Table 4

Ca/Si ratios for selected stellar environments and Solar System materials are compared to the bulk Ca/Si ratio of the condensing Ca–SiO–H₂–O₂ vapor

Sources	Ca/Si	References
Chondritic solar value	0.06	Anders and Grevesse (1989)
Chondritic aggregate IDPs	0.05	Rietmeijer (1998)
Type I carbonaceous meteorites	0.07	Schramm et al. (1989)
Comet 9P/Tempel 1	0.05–0.06	Lisse et al. (2007)
Solar photosphere	0.05	Ross and Aller (1976)
Field B stars	0.107	Snow and Witt (1996)
Disk F, G stars	0.06	Snow and Witt (1996)
Globular cluster M13	0.25; 0.4	Behr et al. (1999)
Bulk Ca–SiO–H ₂ –O ₂ vapor	0.4	This work

stead there is a deficiency of condensates. The condensates, e.g. CaSiO₃ (amorphous wollastonite), that originally clustered in the central region of the diagram reacted with condensing and condensed grains on mixing lines 1–3 (Fig. 5; arrows). In this manner, condensing and growing grains (fusion) obtained the compositions matching the two intermediate DME compositions, average Ca/(Ca + Si) (atomic) at 42 and 72 (Table 2), matching those in the CaO–SiO₂ system (Fig. 4).

This condensation experiment on a refractory vapor is the first time we find a deep metastable eutectic phase that has a stoichiometric calciosilica mineral composition, i.e. CaSiO₃, but is an amorphous solid. It is the result of the equilibrium CaO–SiO₂ phase relationships wherein Ca-olivine, larnite (Ca₂SiO₄), melts at high temperature. This finding is significant because it is the first example of a highly reactive, stoichiometric amorphous condensate that, because of its stoichiometric composition, would easily crystallize to a refractory mineral in astronomical vapor-condensation environments, e.g., supersaturated stellar outflows (Nuth and Hecht, 1990). Amorphous calciosilica grains with a stoichiometric composition set the stage for a diversity of Ca-refractory dust mineralogy. Such minerals were identified in 81P/Comet Wild 2 (Zolensky et al., 2006) wherein they were interpreted as support for long-range dust transport from the inner solar nebula to the Kuiper belt comet-accretion region (Brownlee et al., 2006). This interpretation presumes that the CAI-like grains formed as thermodynamically stable minerals. We note that wollastonite (CaSiO₃) whiskers that are an unique condensation growth morphology are present inside cavities in the Allende meteorite (Miyamoto et al., 1979; Barber et al., 1984).

4.1. Astronomical implications

During non-equilibrium vapor condensation the bulk Mg/Si, Fe/Si, Al/Si, or Ca/Si ratio of the condensing vapor will not affect the fundamental deep metastable eutectic nature of the condensates that invariably occur with all of the possible DME compositions. The bulk ratio only affects the relative proportions for each of the possible DME dust grains (Rietmeijer et al., 2004). The Ca/Si ratios of chondritic aggregate IDPs, CI carbonaceous meteorites, Comet 9P/Tempel 1 (Lisse et al., 2007) and the solar photosphere are very similar (Table 4). A stellar abundance may serve as a proxy of the condensing circumstellar vapor composition. For the solar (or chondritic) ratio, the

Ca–SiO–H₂–O₂ vapor condensation experiment predicts that kinetically controlled solar nebula condensation would yield mainly pure silica and low-Ca, CaSiO dust resembling condensed calciosilica grains of the first population in Table 2 and Ca₆Si₈O₂₂ (smectite dehydroxylate; second population; Table 2). The similar Ca/Si ratios for solar, Field B, Disk F and G stars (Table 4) suggest these stars could be surrounded by solar system-like calciosilica dust. The Ca/Si ratios in Globular Cluster M13 (Table 4) suggest that condensing Ca–SiO–H₂–O₂ vapors would produce calciosilica dust of all four DME compositions.

Condensed dust-aging could ultimately lead to stoichiometric crystalline dust (Fabian et al., 2000; Hallenbeck et al., 2000; Thompson and Tang, 2001; Rietmeijer et al., 2002b) but aging of grains <100 nm will initially lead to metastable mineral assemblies due to the surface free energy contribution to the overall energy budget (Rietmeijer et al., 1986). The calciosilica minerals that could be present in Globular Cluster M13 as a result of DME condensate dust-aging might include

- (1) Wollastonite, CaSiO₃ (a pyroxene mineral), from the decomposition of amorphous Ca-smectite dehydroxylate dust, viz.



- (2) Larnite (Ca₂SiO₄) after crystallization of amorphous condensates with Ca/(Ca + Si) = 0.65,
- (3) Hatrurite (Ca₃SiO₅) + CaO (lime) from the aging of CaSiO condensates with Ca/(Ca + Si) = 0.85.

Solid-state disproportion reactions, solid–solid reactions in aggregates and solid–gas reactions involving highly reactive amorphous DME dust condensates will proceed more rapidly than reactions among crystalline solids of the same composition because, all other parameters being equal, no crystal bonds need to be broken in amorphous solids.

4.2. Diopside (MgCaSi₂O₆) formation

Diopside, MgCaSi₂O₆ (a pyroxene mineral) is observed around protostars and in O-rich planetary nebulae (Molster and Waters, 2003; Chiavassa et al., 2005), in Comets 81P/Wild 2 (Zolensky et al., 2006) and 9P/Tempel 1 (Lisse et al., 2006), and in aggregate IDPs (Rietmeijer, 1999). Its complex chemical composition could be the result of thermal annealing (aging) of mixed amorphous grains that consisted of DME smectite dehydroxylate and amorphous CaSiO₃ condensates, viz.



Alternatively, and much more likely, diopside could result from the annealing of mixed enstatite and amorphous CaSiO₃ condensate grains, viz.

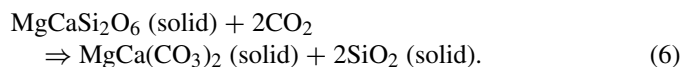


as enstatite is present in active comets, e.g. Comet Hale–Bopp (Wooden et al., 1999).

4.3. Carbonate formation

The apparent co-occurrence of diopside and dolomite, and MgFe-silicates and MgFe-carbonates, cannot be coincidental. Carbonate formation could be associated with the processes that produced these silicate minerals. Calcite and dolomite were reported in planetary nebula NGC 6302 (Kemper et al., 2002). Calcite was found around the protostar NGC 1333-IRS 4 (Ceccarelli et al., 2002), and around low and intermediate mass protostars (Chiavassa et al., 2005). Chiavassa et al. (2005) noted that variations in their spectral features could be attributed to small amounts of impurity elements (Si, Fe, Mg), the dust-forming process, the history of the dust or its temperature. Carbonate, specifically calcite, absent the presence of liquid water could be from (1) direct condensation from gaseous CO₂ and CaO, (2) interactions between an accreted interstellar ice mantle containing CO₂ either dissolved or trapped in the ice, with its underlying silicate core when heating by incident X-rays increased the mobility of molecules in the water-ice mantle to a point where a monolayer or so of liquified water could exist for hydrocryogenic alteration (Rietmeijer, 1985), or (3) an indirect process of silicate interacting with gaseous H₂O to form hydrogenated silicate that later reacted with CO₂ to form carbonates (Kemper et al., 2002; Ceccarelli et al., 2002; Chiavassa et al., 2005). Toppani et al. (2005) tested this reaction experimentally by condensing amorphous silicates from a “solar composition vapor” (AlCa-bearing magnesiosilica vapor) and a MgO-containing Ca,Al,SiO vapor in a CO₂–H₂O-rich vapor wherein they produced complex hydrated carbonates via non-equilibrium condensation. Thermal annealing of the condensates produced Ca-rich carbonate nanocrystals (Toppani et al., 2005). This two-step scenario lowers the probability that this carbonate-forming process will be efficient. We submit that amorphous solids will react with gaseous CO₂ and H₂O leading to the formation of carbonates (e.g., Chiavassa et al., 2005) or hydrated silicates (e.g., Malfait et al., 1999).

Amorphous or crystalline diopside grains when reacting with CO₂ might produce dolomite, viz.



When CO instead of CO₂ was involved, the reaction would yield dolomite + SiO, a stable gas phase molecule (Nuth and Donn, 1984). This carbonate-forming reaction will be sensitive to the CO₂/CO ratio that determines the SiO_(gas)/silica_(solid) ratio for the reaction products. Unlike dolomite, calcite (CaCO₃) is common in astronomical environments and its formation mechanism should be relatively efficient (Chiavassa et al., 2005). The finding of CaSiO₃ condensates that formed during Ca–SiO–H₂–O₂ vapor condensation allows a very simple, single-step reaction of amorphous CaSiO₃ condensates, viz.



This reaction will be independent of the presence of precursor solids in low-H₂O or H₂O-free environments. It predicts that when this reaction has run its full course in the environments wherein calcite was detected there should also be silica

grains. In fact, the presence of silica dust in planetary nebula NGC 6302 and around protostar NGC 1333-IRS 4 might be evidence that this carbonate-forming reaction from an amorphous refractory Ca-silicate dust precursor had occurred. The other reactions we indicated are similarly testable by searches for co-occurring silica dust or its crystalline polymorphs. Although these reactions are speculative, they are rooted in the data obtained from this refractory vapor phase condensation experiment. Thus we predict that phases such as pure lime (CaO) should not be a direct, vapor phase condensate but might instead be a product of dust-aging, as would be the Ca-olivine larnite. These hypotheses could be verified by appropriate astronomical searches in systems where extensive dust processing may have occurred. The above predictions were derived from the results of the Ca–SiO–H₂–O₂ vapor condensation experiment and they do not consider other parameters, e.g. ultraviolet input, to these chemical reactions.

5. Conclusions

The formation of highly disordered, amorphous, nanometer dust condensates during kinetically controlled condensation of a Ca–SiO–H₂–O₂ vapor was entirely constrained by the predictable deep metastable eutectic points in the Ca–Si (at) and the SiO₂–CaO phase diagrams. The amorphous calciosilica condensates occurred with all four deep metastable eutectic compositions that typically do not match compositions of stoichiometric minerals. We report the first observation of a DME condensate that, although amorphous, does have the stoichiometric Ca-olivine composition. We discuss implications for the formation of refractory Ca-silicates, e.g. wollastonite, diopside and larnite, normally considered to be high-temperature mineral condensates, by thermally supported reactions of amorphous calciosilica condensates. We offer pathways for the formation of dolomite and calcite by reactions of amorphous calciosilica dust with CO₂ or even CO and we offer observable constraints for these reactions, including the SiO_(gas)/silica_(solid) ratio and the presence of silica dust (amorphous or crystalline) that is a common byproduct of thermal aging of circumstellar calciosilica dust just as it is a marker for the aging of condensed magnesian silica dust (Rietmeijer et al., 1986, 2002b). We submit a cornucopia of Ca-minerals that should be considered for future spectroscopic surveys, e.g. using the Spitzer Space telescope. Future laboratory analyses of 81P/Wild 2 dust may reveal many of these Ca-silicates and Ca-bearing silicates and carbonates in this Jupiter-family comet. Finally, Wickramasinghe (1971) had proposed that irradiated quartz grains could explain some of the interstellar extinction features albeit that condensation of a pure silica phase was considered to be unlikely. Silica produced by circumstellar dust-aging alleviates the earlier restriction but it cannot be used as proof of the earlier contention.

Acknowledgments

F.J.M.R. and A.P. acknowledge grant NNG04GM48A from the NASA Goddard Space Flight Center. J.A.N. is grateful for the support he has received from the Cosmochemistry Program

at NASA Headquarters. HRTEM analyses were performed in the Electron Microbeam Analyses Facility in the Department of Earth and Planetary Sciences (UNM) where Dr. Ying-Bing Jiang provided technical assistance.

References

- Aasland, S., McMillan, P.F., 1994. Density-driven liquid–liquid phase separation in the system Al₂O₃–Y₂O₃. *Nature* 369, 633–636.
- Anders, E., Grevesse, N., 1989. Abundances of the elements: Meteoritic and solar. *Geochim. Cosmochim. Acta* 53, 197–214.
- Barber, D.J., Martin, P.M., Hutcheon, I.D., 1984. The microstructure of minerals in coarse-grained Ca–Al-rich inclusions from the Allende meteorite. *Geochim. Cosmochim. Acta* 48, 769–783.
- Behr, B.B., Cohen, J.G., McCarthy, J.K., Djorgovski, S.G., 1999. Striking photospheric abundance anomalies in blue horizontal-branch stars in globular cluster M131. *Astrophys. J.* 517, L135–L138.
- Bouwman, J., Meeus, G., de Koter, A., Hony, S., Dominik, C., Waters, L.B.F.M., 2001. Processing of silicate dust grains in Herbig Ae/Be systems. *Astron. Astrophys.* 375, 950–962.
- Brearely, A.J., Jones, R.H., 1998. Chondritic meteorites. In: Papike, J.J. (Ed.), *Reviews in Mineralogy*, vol. 36. Mineralogical Society of America, Chantilly, VA, pp. 3–1–3–398.
- Brownlee, D., and 184 colleagues, 2006. Comet 81P/Wild 2 under a microscope. *Science* 314, 1711–1716.
- Ceccarelli, C., Caux, E., Tielens, A.G.G.M., Kemper, F., Waters, L.B.F.M., Phillips, T., 2002. Discovery of calcite in the solar type protostar NGC 1333-IRAS 4. *Astron. Astrophys.* 395, L29–L33.
- Chiavassa, A., Ceccarelli, C., Tielens, A.G.G.M., Caux, E., Maret, S., 2005. The 90–110 μm dust feature in low to intermediate mass protostars: Calcite? *Astron. Astrophys.* 432, 547–557.
- Cliff, G., Lorimer, G.W., 1975. The quantitative analysis of thin specimens. *J. Microsc.* 103, 203–207.
- Ehlers, E.G. (Ed.), 1972. *The Interpretation of Geological Phase Diagrams*. Freeman, San Francisco, 280 pp.
- De, B.R., 1979. Disequilibrium condensation environments in space: A frontier in thermodynamics. *Astrophys. Space Sci.* 65, 191–198.
- Fabian, D., Jäger, C., Henning, Th., Dorschner, J., Mutschke, H., 2000. Steps toward interstellar silicate mineralogy. V. Thermal evolution of amorphous magnesium silicates and silica. *Astron. Astrophys.* 364, 282–292.
- Fegley Jr., B., 2000. Kinetics of gas-grain reactions in the solar nebula. *Space Sci. Rev.* 92, 177–200.
- Greshake, A., Bischoff, A., Putnis, A., 1998. Transmission electron microscope study of compact type A calcium–aluminum-rich inclusions from CV3 chondrites: Clues to their origin. *Meteorit. Planet. Sci.* 33, 75–87.
- Grossman, L., Larimer, J.W., 1974. Early chemical history of the Solar System. *Rev. Geophys. Space Phys.* 1, 71–101.
- Hallenbeck, S.L., Nuth III, J.A., Daukantes, P.L., 1998. Mid-infrared spectral evolution of amorphous magnesium silicate smokes annealed in vacuum: Comparison to cometary spectra. *Icarus* 131, 198–209.
- Hallenbeck, S.L., Nuth III, J.A., Nelson, R.A., 2000. Evolving optical properties of annealing silicate grains: From amorphous condensate to crystalline mineral. *Astrophys. J.* 535, 247–255.
- Harker, D.E., Woodward, C.E., Wooden, D.H., 2005. The dust grains from 9P/Tempel 1 before and after the encounter with Deep Impact. *Science* 310, 278–280.
- Highmore, R.J., Greer, A.L., 1989. Eutectics and the formation of amorphous alloys. *Nature* 339, 363–365.
- Hill, H.G.M., Grady, C.A., Nuth III, J.A., Hallenbeck, S.L., Sitko, M.L., 2001. Constraints in nebular dynamics and chemistry based on observations of annealed magnesium silicate grains in comets and in disks surrounding Herbig Ae/Be stars. *Proc. Natl. Acad. Sci.* 98, 2182–2187.
- Kemper, F., Jäger, C., Waters, L.B.F.M., Henning, Th., Molster, F.J., Barlow, M.J., Lim, T., de Koter, A., 2002. Detection of carbonates in dust shells around evolved stars. *Nature* 415, 295–297.
- Kimura, Y., Nuth III, J.A., 2005. Laboratory synthesized calcium oxide and calcium hydroxide grains: A candidate to explain the 6.8 μm band. *Astrophys. J.* 630, 637–640.

- Kozasa, T., Sogawa, H., 1997. Formation of dust grains in circumstellar envelopes of oxygen-rich AGB stars. *Astrophys. Space Sci.* 251, 165–170.
- Lisse, C.M., and 16 colleagues, 2006. Spitzer spectral observations of the Deep Impact ejecta. *Science* 313, 635–640.
- Lisse, C.M., Kraemer, K.E., Nuth III, J.A., Li, A., Joswiak, D., 2007. Comparison of the composition of the Tempel 1 ejecta to the dust in Comet C/Hale–Bopp 1995 O1 and YSO HD 100546. *Icarus* 187, 69–86.
- Malfait, K., Waelkens, C., Bouwman, J., de Koter, A., Waters, L.B.F.M., 1999. The ISO spectrum of the young star HD 142527. *Astron. Astrophys.* 345, 181–186.
- Miyamoto, M., Onuma, N., Takeda, H., 1979. Wollastonite whiskers in the Alende meteorite and their bearing on a possible post-condensation process. *Geochem. J.* 13, 1–5.
- Molster, F.J., Waters, L.B.F.M., 2003. The mineralogy of interstellar and circumstellar dust. In: Henning, Th. (Ed.), *Astromineralogy Lecture Notes in Physics*, vol. 609. Springer, Heidelberg, pp. 121–170.
- Nelson, R., Thieme, M., Nuth, J., Donn, B., 1989. Oxygen isotopic fractionation in the condensation of refractory smokes. *Proc. Lunar Sci. Conf.* 19, 559–563.
- Nuth, J.A., Donn, B., 1982. Experimental studies of the vapor phase nucleation of refractory compounds. 1. The condensation of SiO. *J. Chem. Phys.* 77, 2639–2646.
- Nuth, J.A., Donn, B., 1984. Thermal metamorphism of Si₂O₃ (a circumstellar dust analog). In: *Proc. 14th Lunar Planet. Sci. Conf. Part 2. J. Geophys. Res. Suppl.* 89, B657–B661.
- Nuth, J.A., Hecht, J.H., 1990. Signatures of aging silicate dust. *Astrophys. Space Sci.* 163, 79–94.
- Nuth III, J.A., Hallenbeck, S.L., Rietmeijer, F.J.M., 1999. Interstellar and interplanetary grains, recent developments and new opportunities for experimental chemistry. In: Ehrenfreund, P., Krafft, K., Kochan, H., Pirronello, V. (Eds.), *Laboratory Astrophysics and Space Research*. Kluwer Academic Publishers, Dordrecht, pp. 143–182.
- Nuth III, J.A., Hill, H.G.M., Kletetschka, G., 2000a. Determining the ages of comets from the fraction of crystalline dust. *Nature* 406, 275–296.
- Nuth III, J.A., Hallenbeck, S.L., Rietmeijer, F.J.M., 2000b. Laboratory studies of silicate smokes: Analog studies of circumstellar materials. *J. Geophys. Res.* 105 (A5), 10387–10396.
- Nuth, J.A., Rietmeijer, F.J.M., Hallenbeck, S.L., Withey, P.A., Ferguson, F., 2000c. Nucleation, growth, annealing and coagulation of refractory oxides and metals: Recent experimental progress and applications to astrophysical systems. In: Sitko, M.L., Sprague, A.L., Lynch, D.K. (Eds.), *Thermal Emission Spectroscopy and Analysis of Dust, Disks and Regoliths*. In: *Astron. Soc. Pacific Conf. Series*, vol. 196. Astronomical Society of the Pacific, San Francisco, pp. 313–332.
- Nuth, J.A., Rietmeijer, F.J.M., Hill, H.G.M., 2002. Condensation processes in astrophysical environments: The composition and structure of cometary grains. *Meteorit. Planet. Sci.* 37, 1579–1590.
- Okamoto, H., 2001. Ca–O (calcium–oxygen). *J. Phase Equilib.* 22 (1), 87.
- Prigogine, I., 1978. Time, structure, and fluctuations. *Science* 201, 777–785.
- Prigogine, I., 1979. Irreversibility and randomness. *Astrophys. Space Sci.* 65, 371–381.
- Rietmeijer, F.J.M., 1985. A model for diagenesis in proto-planetary bodies. *Nature* 313, 293–294.
- Rietmeijer, F.J.M., 1988. Sulfides and oxides in comets. *Astrophys. J.* 331, L137–L138.
- Rietmeijer, F.J.M., 1990. Salts in two chondritic porous interplanetary dust particles. *Meteoritics* 25, 209–214.
- Rietmeijer, F.J.M., 1992. Nonequilibrium iron-oxide formation in some low-mass post-asymptotic giant branch stars. *Astrophys. J.* 400, L39–L41.
- Rietmeijer, F.J.M., 1998. Interplanetary dust particles. In: Papike, J.J. (Ed.), *Reviews in Mineralogy*, vol. 36. Mineralogical Society of America, Chantilly, VA, pp. 2–1–2–95.
- Rietmeijer, F.J.M., 1999. Metastable non-stoichiometric diopside and Mg-wollastonite: An occurrence in an interplanetary dust particle. *Am. Mineral.* 84, 1883–1894.
- Rietmeijer, F.J.M., 2002. The earliest chemical dust evolution in the solar nebula. *Chem. Erde* 62, 1–45.
- Rietmeijer, F.J.M., Karner, J.M., 1999. Metastable eutectic gas to solid condensation in the Al₂O₃–SiO₂ system. *J. Chem. Phys.* 110, 4554–4558.
- Rietmeijer, F.J.M., Nuth, J.A., 1991. Tridymite and maghémite formation in a Fe–SiO smoke. *Proc. Lunar Sci. Conf.* 21, 591–599.
- Rietmeijer, F.J.M., Nuth III, J.A., 2000. Metastable eutectic equilibrium brought down to Earth. *Eos Trans. AGU* 81 (36), 414–415.
- Rietmeijer, F.J.M., Nuth III, J.A., 2002. Experimental astromineralogy: Circumstellar ferromagnesian silicate dust in analogs and natural samples. In: Green, S.F., Williams, I.P., McDonnell, J.A.M., McBride, N. (Eds.), *Dust in the Solar System and Other Planetary Systems*. In: *COSPAR Colloquia Series*, vol. 15. Elsevier Science, Oxford, UK, pp. 333–339.
- Rietmeijer, F.J.M., Nuth III, J.A., 2004. Grain sizes of ejected comet dust: Condensed dust analogs, interplanetary dust particles and meteors. In: Colanagli, L., Mazzotta Epifani, E., Palumbo, P. (Eds.), *The New ROSETTA Targets—Observation, Simulations and Instrument Performances*. In: *Astrophys. Space Sci. Library*. Kluwer Academic Publishers, Dordrecht, pp. 97–110.
- Rietmeijer, F.J.M., Nuth, J.A., Mackinnon, I.D.R., 1986. Analytical electron microscopy of Mg–SiO smokes: Comparison with XRD and infrared studies. *Icarus* 65, 211–222.
- Rietmeijer, F.J.M., Nuth III, J.A., Karner, J.M., 1999a. Metastable eutectic gas to solid condensation in the FeO–Fe₂O₃–SiO₂ system. *Phys. Chem. Chem. Phys.* 1, 1511–1516.
- Rietmeijer, F.J.M., Nuth III, J.A., Karner, J.M., 1999b. Metastable eutectic condensation in a Mg–Fe–SiO–H₂–O₂ vapor: Analogs to circumstellar dust. *Astrophys. J.* 527, 395–404.
- Rietmeijer, F.J.M., Nuth III, J.A., Karner, J.M., Hallenbeck, S.L., 2002a. Gas to solid condensation in a Mg–SiO–H₂–O₂ vapor: Metastable eutectics in the MgO–SiO₂ phase diagram. *Phys. Chem. Chem. Phys.* 4, 546–551.
- Rietmeijer, F.J.M., Hallenbeck, S.L., Nuth III, J.A., Karner, J.M., 2002b. Amorphous magnesiosilicate smokes annealed in vacuum: The evolution of magnesium silicates in circumstellar and cometary dust. *Icarus* 156, 269–286.
- Rietmeijer, F.J.M., Nuth III, J.A., Nelson, R.N., 2004. Laboratory hydration of condensed magnesiosilicate smokes with implications for hydrated silicates in IDPs and comets. *Meteorit. Planet. Sci.* 39, 723–746.
- Rietmeijer, F.J.M., Nuth III, J.A., Rochette, P., Marfaing, J., Pun, A., Karner, J.M., 2006. Deep metastable eutectic condensation in Al–Fe–SiO–O₂–H₂ vapors: Implications for natural Fe-aluminosilicates. *Am. Mineral.* 91, 1688–1698.
- Ross, J.E., Aller, L.H., 1976. The chemical composition of the Sun. *Science* 191, 1223–1229.
- Schramm, L.S., Brownlee, D.E., Wheelock, M.M., 1989. Major element composition of stratospheric micrometeorites. *Meteoritics* 24, 99–112.
- Sitko, M.L., Lynch, D.K., Russell, R.W., Hanner, M.S., 2004. 3–14 micron spectroscopy of Comets C/2002 04 (Hönl), C/2002 V1 (NEAT), C/2002 X5 (Kudo–Fujikawa), C/2002 Y1 (Juels–Holvorcem), and 69P/Taylor and the relationships among grain temperature, silicate band strength, and structure among comet families. *Astrophys. J.* 612, 576–587.
- Snow, T.P., Witt, A.N., 1996. Interstellar depletions updated: Where all the atoms went. *Astrophys. J.* 468, L65–L68.
- Sosman, R.B., 1955. New and old phases of silica. *Trans. Br. Ceram. Soc.* 54, 655–670.
- Thompson, S.P., Tang, C.C., 2001. Laboratory investigation of crystallization in annealed amorphous MgSiO₃. *Astron. Astrophys.* 368, 721–729.
- Toppani, A., Robert, F., Libourel, G., de Donato, Ph., Bares, O., d’Hendecourt, L., Ghanbaja, J., 2005. A ‘dry’ condensation origin of circumstellar carbonates. *Nature* 437, 1121–1124.
- Wickramasinghe, N.C., 1971. Irradiated quartz particles as interstellar grains. *Nat. Phys. Sci.* 234, 7–10.
- Wood, J.A., 1988. Chondritic meteorites and the solar nebula. *Annu. Rev. Earth Planet. Sci.* 16, 53–72.
- Wood, J.A., Hashimoto, A., 1993. Mineral equilibrium in fractionated nebular systems. *Geochim. Cosmochim. Acta* 57, 2377–2388.
- Wooden, D.H., Harker, D.E., Woodward, C.E., Butner, H.M., Koike, C., Wittborn, F.C., McMurtry, C.W., 1999. Silicate mineralogy, of the dust in the inner coma of Comet C/1995 O1 (Hale–Bopp) pre- and post-helion. *Astrophys. J.* 517, 1034–1058.

Wynnyckyj, J.R., 1972. Correlations between temperature/composition and pressure/temperature equilibrium diagrams. *High Temp. Sci.* 4, 205–211.

Wynnyckyj, J.R., Pidgeon, L.M., 1972. Investigations on the constitution of the calcium–silicon system. *High Temp. Sci.* 4, 192–204.

Zolensky, M.E., 1987. Refractory interplanetary dust particles. *Science* 237, 1466–1468.

Zolensky, M.E., and 74 colleagues, 2006. Mineralogy and petrology of Comet Wild 2 nucleus samples. *Science* 314, 1735–1739.